Electronic Supplementary Material (ESI) for ChemComm.

Emission Enhancement and High Sensitivity of π-Conjugated Dye toward Pressure: Synergistic Effects of Charge-Transfer Excited State and H-Aggregation

Zhanghua Sun,[a,b†] Qiguang Zang,[b†] Qing Luo,[a] Chunyang Lv,[b] Feng Cao,[b] Qingbao Song,[*a] Ruiyang Zhao,[c] Yujian Zhang,[*b] and Wai-Yeung Wong[*d]

[a] College of Chemical Engineering, Zhejiang University of Technology, Caowang Road No. 18, Hangzhou 310000, P. R. China,
E-mail: qbsong@zjut.edu.cn

[b] Department of Materials Chemistry, Huzhou University, East 2nd Ring Rd. No.759, Huzhou, 313000, P. R. China.
E-mail: sciencezyj@foxmail.com

[c] College of Chemical Engineering, Qingdao University of Science and Technology, Qingdao, 266042, P. R. China.

[d] Department of Applied Biology and Chemical Technology, The Hong Kong Polytechnic University, Hung Hom, Hong Kong, P.R. China.
E-mail: wai-yeung.wong@polyu.edu.hk

† The authors contributed equally to this manuscript.

Experimental section

Materials: 4-(Diphenylamino)phenylboronic acid, 7-bromobenzo[c][1,2,5]thia diazole-4-carbaldehyde and 3,5-dimethoxyphenylacetonitrile were purchased from Alfa Aesar Co. Ltd. Other reagents were obtained from Sigma-Aldrich or Aladdin Chemicals and used without further purification. Solvents were purified according to standard laboratory methods.

Instrumentation: ^{1}H NMR and ^{13}C NMR of triazole derivatives were recorded on a Brüker AM500 spectrometer using tetramethylsilane (TMS, δ=0 ppm) as internal standard. The time-resolved PL decay spectra of the samples were also performed on an Edinburgh FLS980 fluorescence spectrometer at room temperature. PL measurements at room temperature were obtained on a SENS-9000 (Gilden Photonics, England). The digital photographs were captured by the 550D digital cameras (Canon, Japan). Absolute PL quantum yields (Φ_{PL}) were determined with a spectrometer C11347 (Hamamatsu, Japan). Powder X-ray diffraction experiments were measured on a Philips X'Pert Pro diffractometer (Netherlands). Measurements were made in a 2θ range of 5-50 ° at room temperature with a step of 0.02 ° (2θ).The scan speed was 2 degree/min. The UV-vis absorption spectra were obtained on a Shimadzu UV-2600 spectrophotometer (Japan).

Theoretical calculations: The geometries of all molecules were fully optimized at the SCF level of theory using the Gaussian 09[6] suite of programs package. The ground state geometries have been optimized by using density functional theory (DFT) at B3LYP/6-31G* level.

Scheme S1 Synthetic routes of BTZA

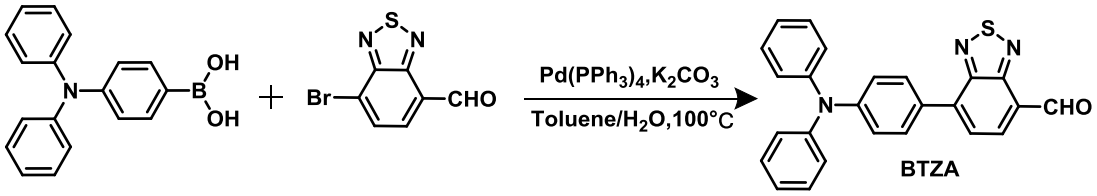

Under an atmosphere of nitrogen, to a mixture of 4-(diphenylamino)phenylboronic acid (6.2 mmol, 1.8 g),7-bromobenzo[c][1,2,5]thiadiazole-4-carbaldehyde (6 mmol, 1.3 g) and $Pd(PPh_3)_4$ (0.22 mmol, 0.25 g) in THF/Toluene (30 mL/50 mL) was added a solution of K_2CO_3 (2.0 M, 1.5 mL) in water, the reaction solution was refluxed overnight. Then the reaction mixture was poured into water, extracted with CH_2Cl_2 and dried over anhydrous Mg_2SO_4. The crude product was purified by column chromatography on silica gel (petroleum ether/DCM = 2/1) to yield **BTZA** (1.8 g, 75%).

^{1}H NMR (400 MHz, $CDCl_3$) δ 10.62 (s, 1H), 9.32 (d, *J* = 7.2 Hz, 1H), 9.04-9.02 (*m*, 3H), 7.39 (t, *J* = 8 Hz, 4H), 7.15 (t, *J* = 8 Hz, 6H), 7.08 (d, *J* = 8.8 Hz, 2H)

^{13}C NMR ($CDCl_3$) δ 188.8, 154.0, 153.9, 149.4, 147.0, 139.9, 132.9, 130.5, 129.5, 129.1, 125.7, 125.6, 125.4, 124.0, 121.9

MS (Maidi-Tof, m/z) Calculated for $C_{35}H_{26}N_4O_2S$ = 407.49, found [M^+] =406.73

Scheme S2 Synthetic routes of BTA-DMeO

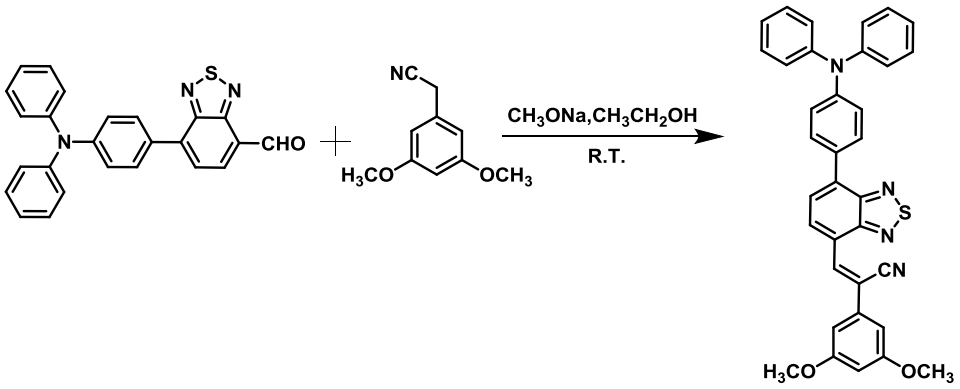

The mixture of **BTZA** (0.82 g, 2 mmol) and 3,5-dimethoxyphenylacetonitrile (0.39 g, 2.2 mmol) in ethanol (HPLC, 40 ml) was stirred at the room temperature for 5 min. Then, a spot of NaOMe were added, and stirred for 5 h. The resulting dye (**BTA-DMeO**) was filtered and repeatedly washed with EtOH solution to give a red powder (0.95g, 82%).

^{1}H NMR (400 MHz, $CDCl_3$) δ 8.71 (d, *J* = 7.6 Hz, 1H), 8.53 (s, 1H), 7.93 (d, *J* = 8 Hz, 2H), 7.83 (s, 1H), 7.31 (t, *J* = 7.6 Hz, 4H), 7.20 (d, *J* = 6 Hz, 6H), 7.09 (s, 2H), 6.95 (d, *J* =2 Hz, 2H), 6.54 (*t*, *J* = 2 Hz, 1H), 3.89 (s, 6H)

^{13}C NMR ($CDCl_3$) δ 161.5, 154.0, 153.4, 147.5, 145.9, 144.8, 136.3, 135.3, 129.6, 128.8, 127.8, 127.2, 126.9, 125.7, 123.2, 119.07, 118.8, 102.8, 99.6, 55.8

MS (Maidi-Tof, m/z) Calculated for $C_{35}H_{26}N_4O_2S$ = 566.68, found [M^+] =565.78,

Scheme S3 Synthetic routes of BTA-MeO

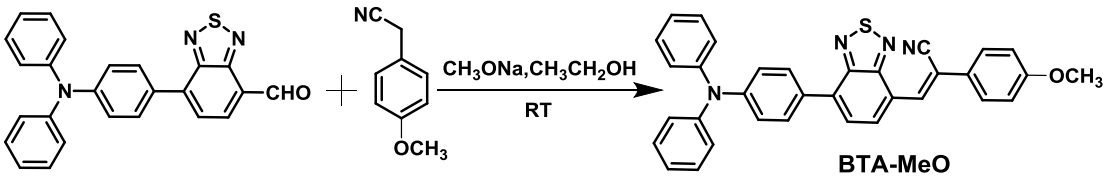

The mixture of **BTZA** (0.3 g, 0.8 mmol) and 4-Methoxyphenylacetonitrile (0.12 g, 0.82 mmol) in ethanol (HPLC, 40 ml) was stirred at the room temperature for 5 min. Then, a spot of NaOMe were added, and stirred for 10 h. The resulting dye (**BTA-MeO**) was filtered and repeatedly washed with EtOH solution to give a red powder (**BTA-MeO**) (0.32 g, 82.5%).

^{1}H NMR (400 MHz, $CDCl_3$) δ 8.67 (d, *J* = 8 Hz, 1H), 8.42 (s, 1H), 7.91 (d, *J* = 8.8 Hz, 2H), 7.81 (d, *J* = 7.6 Hz, 1H), 7.76 (d, *J* = 8.8 Hz, 2H), 7.31 (t, *J* = 7.6 Hz, 4H), 7.22-7.19 (*m*, 6H), 7.09 (t, *J* = 7.2 Hz, 2H), 7.01 (d, *J* = 8.8 Hz, 2H), 3.88 (s, 3H)

^{13}C NMR ($CDCl_3$) δ 160.8, 155.1, 153.2, 148.7, 147.3, 135.2, 133.3, 130.1, 129.9, 129.4, 127.7, 127.6, 126.9, 126.8, 125.2, 123.6, 122.4, 118.3, 114.6, 112.3, 55.5

MS (Maidi-Tof, m/z) Calculated for $C_{34}H_{24}N_4OS$ = 536.65, found [M^+] =535.78,

Table S1. Crystal data and structure refinement for crystals BZA-DMeO and BZA-MeO

Samples	**BTA-DMeO (CCDC: 1902104)**	**BTA-MeO (CCDC: 1902106)**
Formula	$C_{35}H_{26}N_4O_2S$	$C_{34}H_{24}N_4OS$
Mr	566.68	536.65
Temperature (K)	100	150
Crystal system	Triclinic	Monoclinic
Space group	P-1	P21/c
a (Å)	7.25705(16)	17.3663(9)
b (Å)	9.16553(18)	15.3052(5)
c (Å)	22.3109(4)	10.2855(5)
α (°)	82.6200(15)	90
β (°)	86.5593(16)	105.704(5)
γ (°)	70.244(2)	90
V(Å^3)	1384.87(5)	2631.8(2)
Z	2	4
D_{calc} (mg/m^3)	1.364	1.359
Theta Range (°)	3.996 - 67.080	3.910 - 73.224
F (000)	596.0	1128
h, *k*, l_{max}	5, 10, 26	21, 16, 6
N_{ref}	11937	14050
T_{min}, T_{max}	0.949, 1.00	0.826, 1.00
Independent reflections	4865	5184
Goodness-of-fit on F^2	1.054	1.090
R_{int}	0.0258	0.0427
$R_1[I>2\sigma(I)]$	0.0341	0.0814
$wR_2[I>2\sigma(I)]$	0.0888	0.2318
R_1(all data)	0.0368	0.0959
wR_2(all data)	0.0905	0.2398
S	1.054	1.090

$R_1 = \Sigma||F_o| - |F_c||/\Sigma|F_o|$, $wR_2 = [\Sigma w(F_o^2 - F_c^2)^2/\Sigma w(F_o^2)^2]^{1/2}$

The change in magnitude of the dipole moment between the ground and excited states, that is, $\Delta\mu = |\mu_e - \mu_g|$ can be estimated using the Lippert–Mataga equation

$$hc(v_a - v_f) = hc(v_a^0 - v_f^0) + \frac{2(\mu_e - \mu_g)^2}{a_0^3} f(\varepsilon, n)$$

Where a_0 is the cavity radius in which the solute resides, estimated to be 6.5 Å. μ_g is the ground-state dipole moment, estimated to be 4.54D (ωB97X at the basis set level of 6-31G**), μ_e is the excited state dipole moment. h and c are Planck's constant and the speed of light, respectively, and $f(\varepsilon, n)$ is the orientation polarizability, defined as

$$f(\varepsilon, n) = \frac{\varepsilon - 1}{2\varepsilon + 1} - \frac{n^2 - 1}{2n^2 + 1}$$

Where ε is the static dielectric constant and n is the optical refractivity index of the solvent. Through the analysis of the fitted line in low-polarity solvents, its corresponding μ_e was calculated to be 10.9 D with the slope of 4366 according to Lippert-Mataga equation. However, in high-polarity solvents, the μ_e was increased to 22.8 D with the slope of 24318.

Table S2 Detailed photophysical data of **BTA-DMeO** in the different solvents

Solvents	f	λ_{abs} nm	λ_{flu} nm	ν_a cm^{-1}	ν_f cm^{-1}	ν_a-ν_f cm^{-1}	Φ_{PL}
Hexane	0.0012	485	576	2.06×10^4	1.74×10^4	3.2×10^3	92.4%
Toluene	0.014	492	623	2.03×10^4	1.61×10^4	4.2×10^3	88.9%
Butyl ether	0.096	489	617	2.04×10^4	1.62×10^4	4.2×10^3	89.4%
Isopropyl ether	0.145	487	630	2.05×10^4	1.59×10^4	4.6×10^3	85.2%
Ethyl ether	0.167	485	643	2.06×10^4	1.56×10^4	5.0×10^3	84.2%
THF	0.210	484	687	2.07×10^4	1.46×10^4	6.1×10^3	49.3%
DCM	0.217	486	700	2.06×10^4	1.43×10^4	6.3×10^3	49.4%
DMF	0.276	482	767	2.07×10^4	1.30×10^4	7.7×10^3	1.5%
Acetonitrile	0.305	469	771	2.13×10^4	1.30×10^4	8.3×10^3	1.4%

Table S3 The photophysical properties of **BTA-DMeO** in different states

Samples	λ_{em} **[nm]**	Φ_{PL}	$\langle\tau\rangle$ **[ns]**	k_r **[s^{-1}]**	k_{nr} **[s^{-1}]**
Dye-doped film	604	76.9%	2.8	2.7×10^8	2.3×10^8
Spin-coated film	687	29.3%	5.1	5.7×10^7	1.4×10^8

$\langle\tau\rangle = \sum A_j\tau_j^2 / \sum A_j\tau_j$, j=1, 2, 3..., $k_r = \eta_{PL}/\langle\tau\rangle$, and $k_{nr} = (1-\eta_{PL})/\langle\tau\rangle$ ×where $\langle\tau\rangle$ is the fluorescence lifetime, Φ_{PL} is the PL quantum yield.

Table S4 PL wavelengths (λ_{man}), PL lifetime, and PLQY of **BTA-DMeO** and **BTA-MeO**

Samples		λ_{max} **[nm]**	$\langle\tau\rangle$ **[ns]**	Φ_{PL}	k_r **[s^{-1}]**
BTA-DMeO	**1 atm**	657	7.0	9%	1.3×10^7
	20 MPa	695	5.3	19.3	3.6×10^7
BTA-MeO	**1 atm**	683	3.7	45.9%	1.2×10^8
	20 MPa	699	4.5	43.6%	9.7×10^7

$\langle\tau\rangle = \sum A_j\tau_j^2 / \sum A_j\tau_j$, j=1, 2, 3..., $\Phi_{PL} = \langle\tau\rangle \times k_r$, where $\langle\tau\rangle$ is the fluorescence lifetime, Φ_{PL} is the PL quantum yield

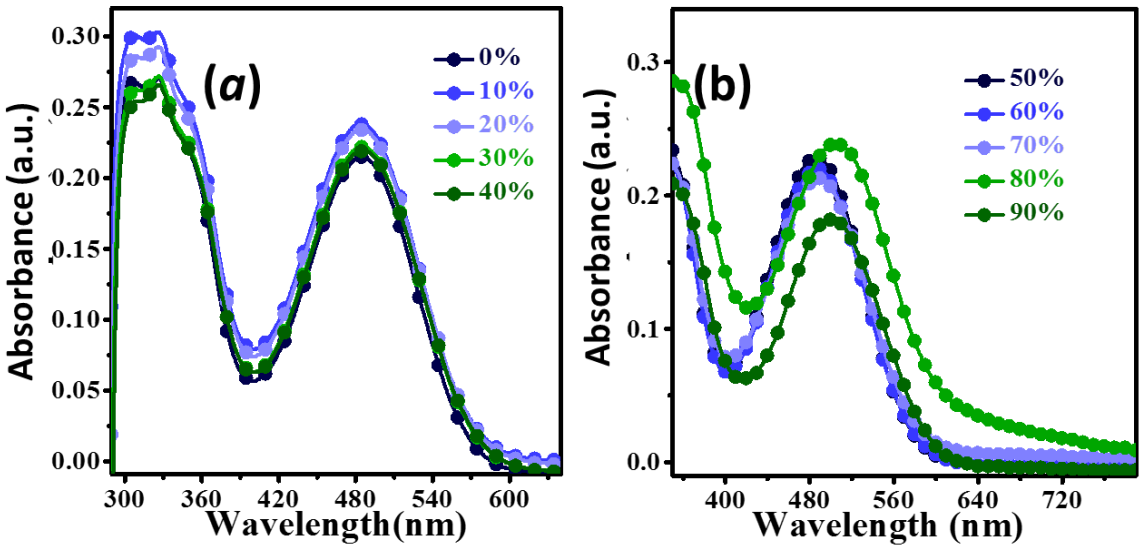

Figure S1 The UV absorption spectra of **BTA-DMeO**, measured in the different solvents with increasing polarity (the orientational polarizability of solvent, Δ*f*, –hexane: 0.0012; toluene: 0.014; butyl ether: 0.096; Isopropyl ether (IPE): 0.145; ethyl ether: 0.167; tetrahydrofuran (THF): 0.210; methylene chloride (DCM): 0.217; N,N-dimethylformamide (DMF): 0.276; and acetonitrile (ACN): 0.305 (**Table S1**, Supporting Information))

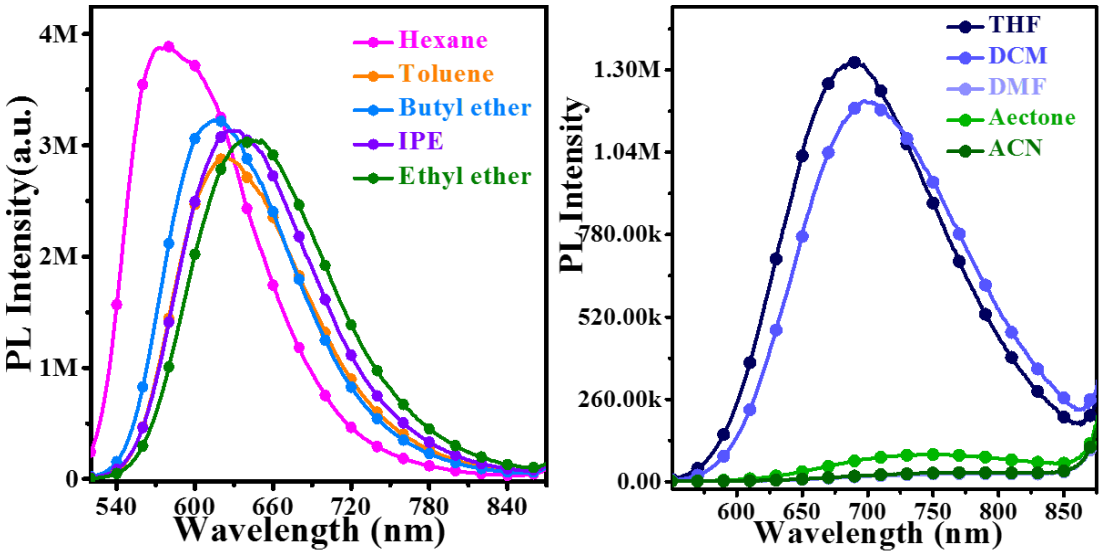

Figure S2 The PL spectra of **BTA-DMeO** in different solvents (10 μM, isopropyl ether (IPE), tetrahydrofuran (THF), N,N-dimethylformamide (DMF), Acetonitrile (ACN) and methylene chloride (DCM)). The excitation wavelength is 500 nm.

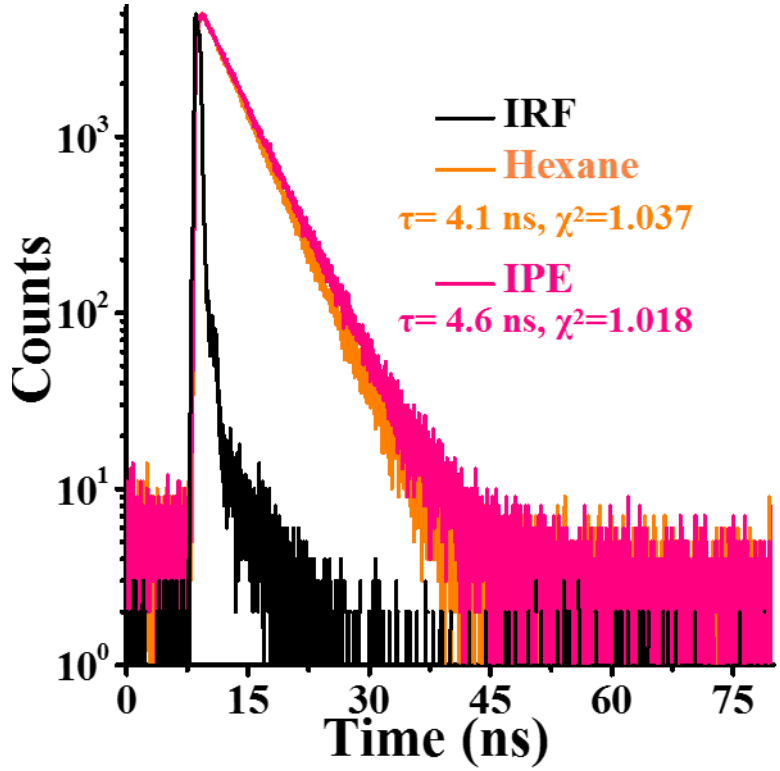

Figure S3 PL lifetime of **BTA-DMeO** in hexane and IPE (10 μM), respectively.

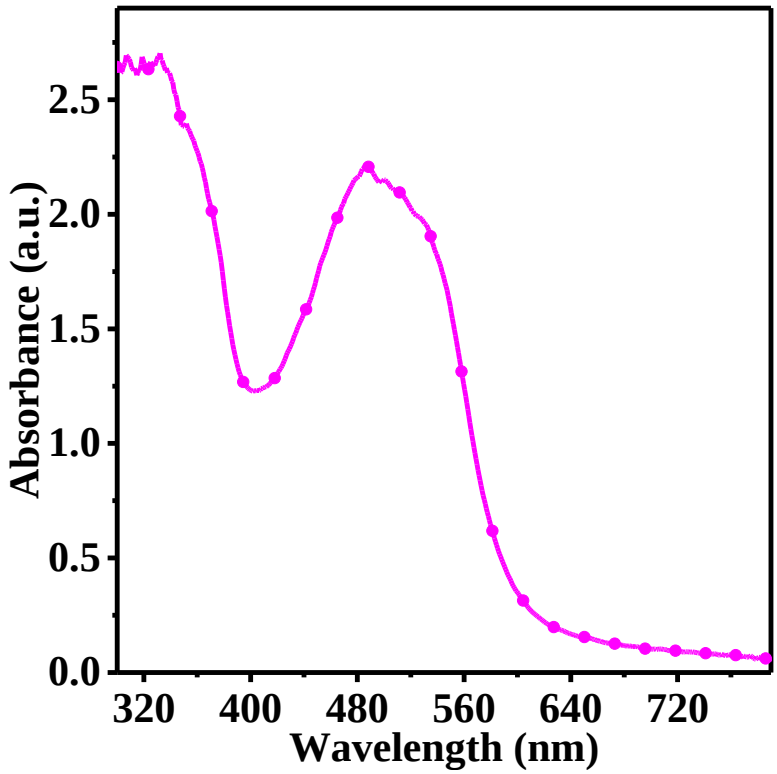

Figure S4 UV-vis absorption spectra of **BTA-DMeO** in the PMMA film.

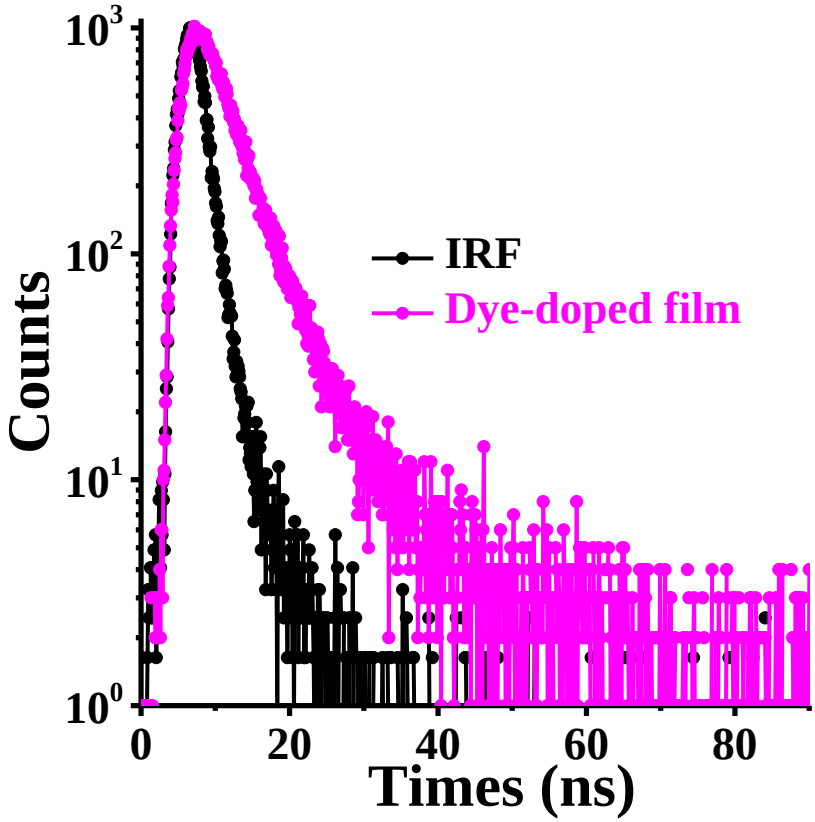

Figure S5 PL lifetime of **BTA-DMeO** in PMMA film.

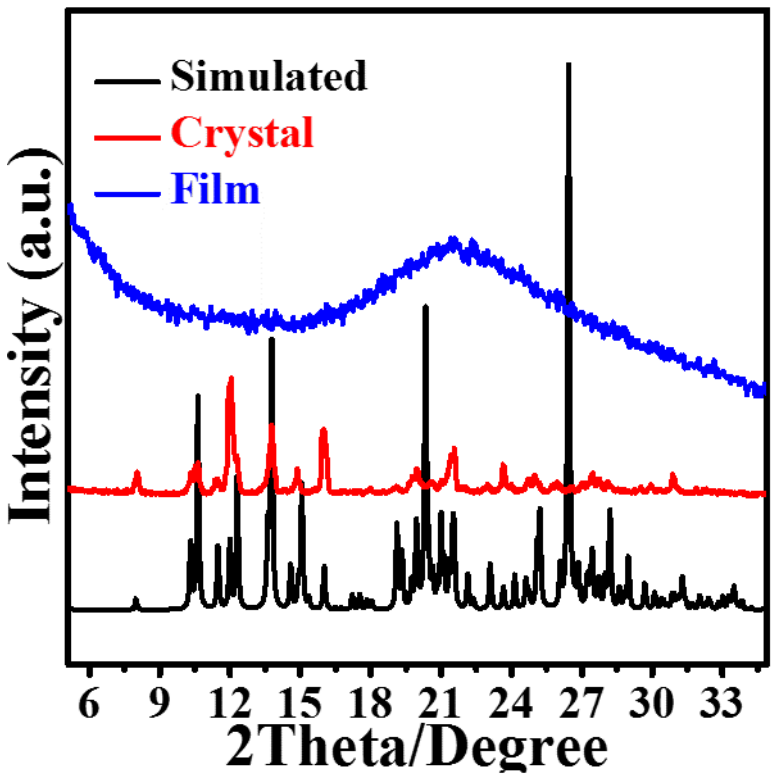

Figure S6 XRD profiles of **BTA-DMeO** in different states;

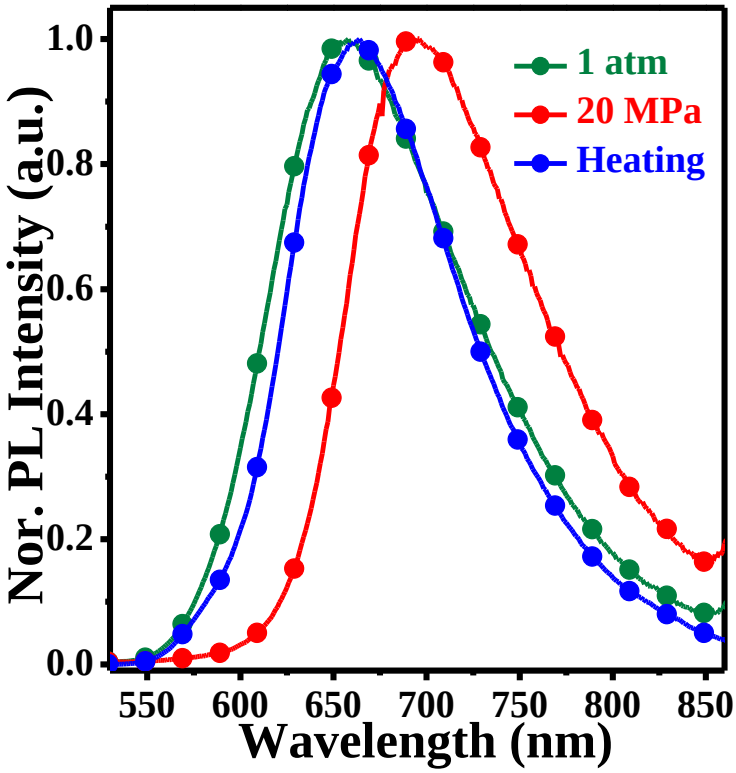

Figure S7 PL spectra of **BTA-DMeO** solid in different states.

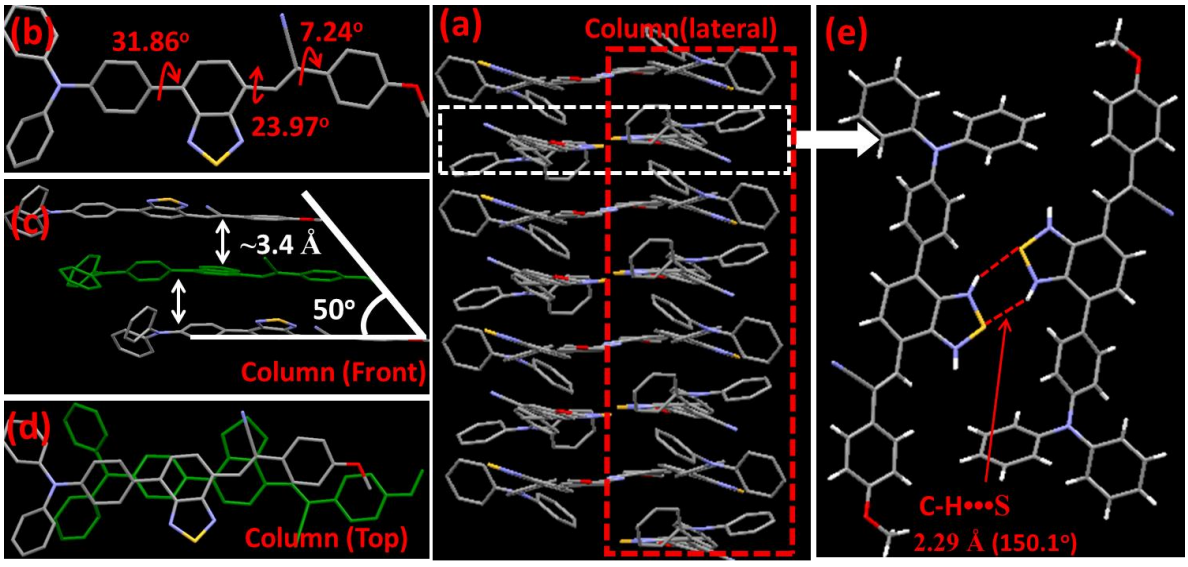

Figure S8 Crystal structures of **BTA-MeO**: (*a*) Lateral view of the column arrangement; (*b*) the dihedral angles of the **BTA-MeO** single-crystal; (*c*) front view of the anti-parallel arrangement along the long molecular axis (3.34 Å); (*d*) top view of the **BTA-MeO** dimer; (e) and illustration of the C–H•••S hydrogen bond interactions.

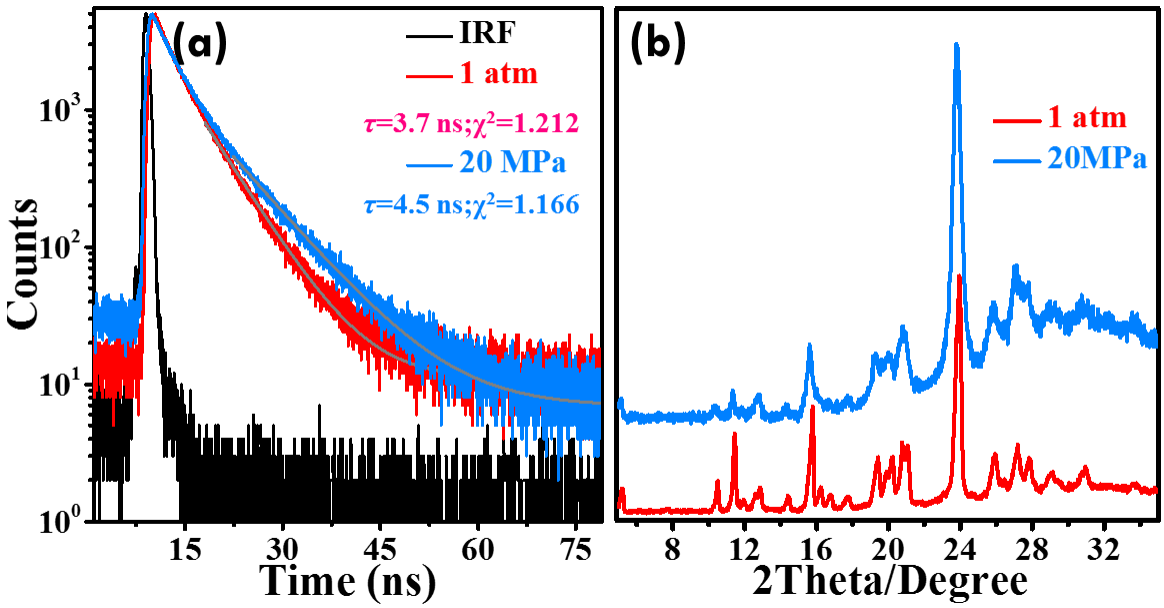

Figure S9 PL lifetime (*a*) and XRD profiles (*b*) of **BTA-MeO** in different states;

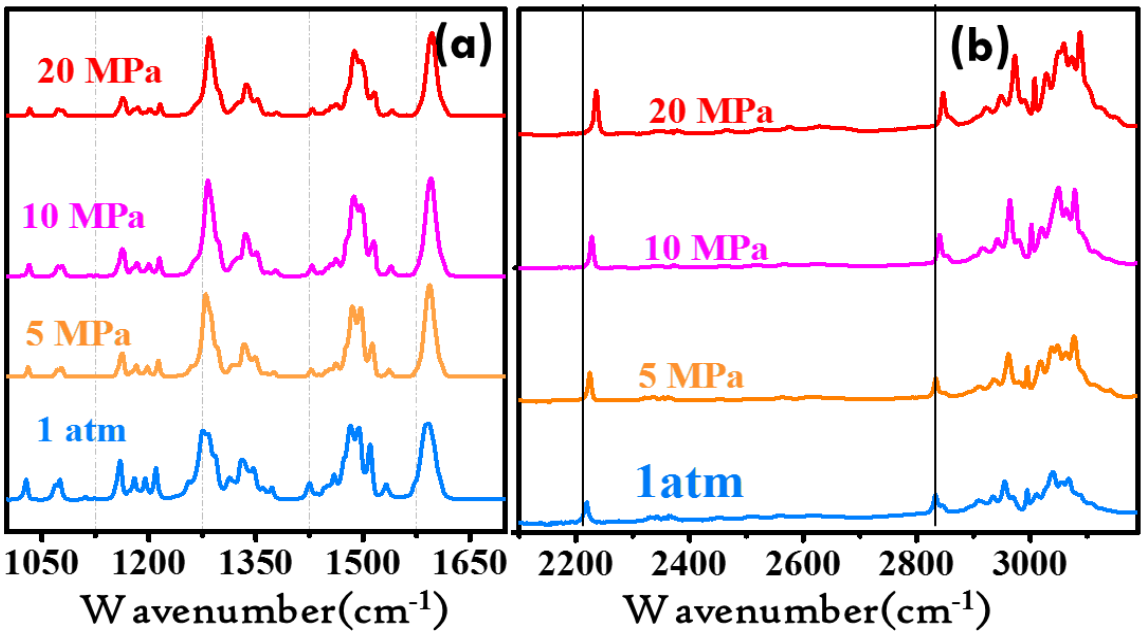

Figure S10 IR spectra of **BTA-DMeO** crystals in the range of 1000–3200 cm^{-1} at various pressures from 1 atm to 20 MPa.

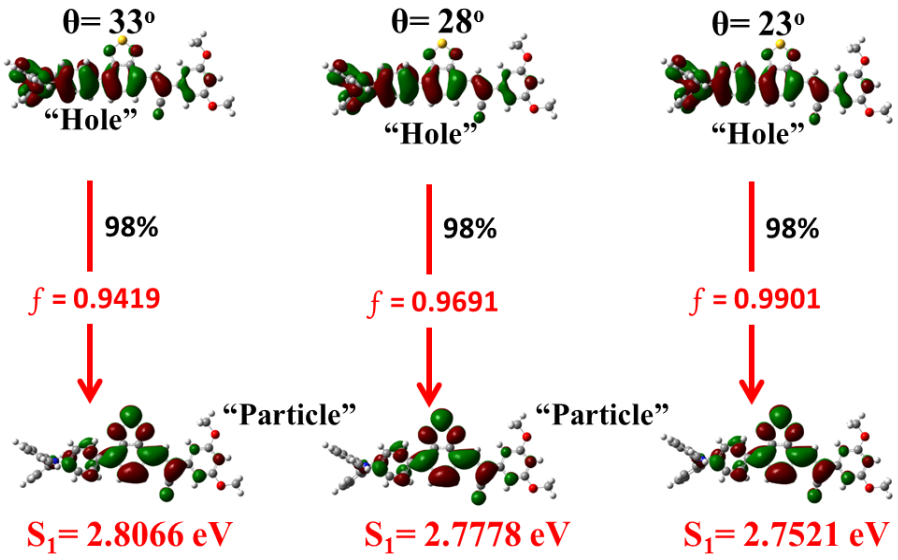

Figure S11 Excitation energies of different **BTA-DMeO** molecular conformations with different dihedral angles (θ_1). The calculations were carried out using the TD/ M06-2X/6-31g (d,p) method, and *f* is the oscillator strength.